Astron. Astrophys. 352, 679–696 (1999)

ASTRONOMY AND ASTROPHYSICS

The evolution of solar granules deduced from 2-D simulations

S.R.O. Ploner[1,2], **S.K. Solanki**[1,2], **and A.S. Gadun**[3]

[1] Institute of Astronomy, ETH-Zentrum, 8092 Zürich, Switzerland
[2] Max-Planck-Institut für Aeronomie, 37191 Katlenburg-Lindau, Germany
[3] Main Astronomical Observatory of Ukrainian NAS, Goloseevo, 252650 Kiev-22, Ukraine

Received 19 May 1999 / Accepted 1 November 1999

Abstract. The evolution of solar granules is investigated on the basis of two dimensional numerical solutions of the hydrodynamic equations describing a compressible, radiatively coupled and gravitationally stratified medium representative of the solar surface layers. The simulation covers 17 Mm on the solar surface and was run for over 5 h of solar time, hence allowing the evolution of over 400 granules to be followed. A statistical investigation of the temporal evolution of granules therefore becomes feasible.

Two types of granules can be distinguished by their means of death: fragmenting and dissolving granules. Properties and average evolutionary histories of these two types of granules are considered. It is found that fragmenting granules are in general large at birth and expand further with time. It is confirmed that fragmentation into two (or more) parts is produced by buoyancy braking, which in turn is initiated by the stronger horizontal flows in larger granules. This last property, finally, is due to mass conservation. The expansion, however, is due to a pressure excess relative to neighbouring granules. The pressure excess is particularly marked if the neighbours are dissolving granules.

In contrast, dissolving granules are born small and shrink before finally disappearing. The shrinkage is caused by their neighbours which generally posses excess gas pressure and larger horizontal flows. In summary, according our findings the fate of a granule is decided by its properties at birth and the company it keeps.

Evidence is presented suggesting that the evolution of both types of granules is driven by events near the solar surface.

Key words: convection – hydrodynamics – methods: numerical – Sun: granulation

1. Introduction

The outer convection zones of the sun and many other cool stars reach up to the solar, respectively stellar surface, rendering their upper boundaries accessible to observations. High resolution images of the solar surface show a pattern of bright granular cells surrounded by dark intergranular lanes. This pattern keeps evolving and granules constantly appear and vanish. The main route to granule death is fragmentation of larger granules into two or more smaller ones (the average number of fragments is 2.8 according to Mehltretter 1978). Less frequent are granules which merge with a neighbour and granules which fade away. The exploding granules are a particularly prominent kind of fragmenting granules (e.g. Title et al. 1989, cf. Rast 1995). They develop a dark centre surrounded by a rapidly expanding bright ring. This route to death is relatively common among large granules and has consequently been well studied observationally. Kawaguchi (1980) found that granules with sizes below $1''$ predominantly dissipate and granules larger than $2''$ fragment. Recently, Karpinsky & Pravdjuk (1998) detected three different size ranges of granules with different fragmentation rates: granules less than 713 km in diameter rarely fragment whereas granules larger than 1200 km show a very high fragmentation rate.

Observations, however, suffer from limited spatial resolution, which adversely affects the study of, in particular, small granules. The fact that time series of homogeneously high resolution images are needed make the observational study of granule evolution especially demanding. In addition, observations only sample the atmospheric layers, whereas the convectively unstable layers are situated below the surface, so that it is unclear from observation alone whether the drivers of granule evolution are situated in atmospheric or deeper layers. Finally, the observed radiation samples physical variables of interest often only indirectly, in many cases non-linearly and always with some averaging along the line-of-sight.

Theory and, in particular, numerical solutions of the fully compressible, radiation-hydrodynamic equations have therefore significantly advanced the understanding of both solar and solar-like convection (see Spruit 1997 for a review). One major result is that granulation is a surface-driven phenomenon. Instead of the older picture of a fluid heated from below the newer view emphasizes the role of the upper boundary which cools the gas and gives rise to strong downdrafts (Stein & Nordlund 1989, 1994, 1998, Nordlund et al. 1997, cf. Rast 1999).

Three dimensional simulations of solar convection have been particularly successful in reproducing observations of spectral line shifts and asymmetries, line widths and granule morphology. (e.g. Dravins et al. 1981, 1986, Nordlund 1985, Wöhl & Nordlund 1985, Lites et al. 1989). Due to their large

Send offprint requests to: S.R.O. Ploner (ploner@astro.phys.ethz.ch)

demand on computational resources, however, they have generally focussed on the behaviour of one or at most a few granules (but see Wöhl & Nordlund 1985), so that the physical properties of granulation have had to be deduced from just a few examples. This makes the results of at least the published 3–D simulations, susceptible to variations from one granule to the next.

Our approach is different. We reduce the spatial dimensions to 2 but simulate instead a part of the solar surface that is sufficiently large to contain approximately 10 granules and follow the evolution of the convection for 5 h of solar time. Hence a large number of granules can be investigated and the statistically significant aspects of their behaviour can be identified and extracted. Although a 2–D model certainly cannot reflect all of the 3–D physics of convection, 2–D simulations are nevertheless able to reproduce many properties of granulation (e.g. Freytag et al. 1996, Gadun et al. 1997, 1998a,b). One advantage of carrying out a statistical study like ours in 2–D instead of 3–D is that many of the quantities (identification of granules and location of fragmentation, averages, etc.) are more straightforward to define in 2–D.

We concentrate on obtaining a better understanding of the physics underlying the evolution of granules. Our investigation differs from the strongly idealized modeling of, e.g., Massaguer et al. (1980) and Hurlburt et al. (1984), who pinpointed the importance of the density stratification (which distinguishes solar convection from laboratory convection) and described buoyancy braking, the mechanism which finally gives rise to new downdrafts inside fragmenting and exploding granules. In simulations including more realistic physics the evolution has been investigated by several authors. Wöhl & Nordlund (1985) calculated the evolution of 65 3–D granules over a time of 138 min, and compared them with observed granules. Stein & Nordlund (1989, 1994) followed the evolution of test particles (corks) over 18 minutes and found that the upflowing gas is smooth whereas the rapid downdrafts are rather inhomogeneous and frequently change the spatial location. Based on idealized numerical experiments Rast (1995) proposed an additional mechanism (besides buoyancy braking) for the creation of downflows. He finds that both in the observations and model calculations the strongest upflows are located close to downflows. While a granule expands the maximum upflows get larger and remain close to the downdrafts. The central part of the granule, however, suffers from an ever weakening upflow, thus providing the condition for a new downdraft. The frequency with which this process occurs remains open.

The structure of this paper is as follows: Sect. 2 introduces the numerical methods, while in Sect. 3 the output of the computations is described and the techniques used to analyze the results are introduced. In Sect. 4 we discuss the evolution of granules and, finally, in Sect. 5 the results and our conclusions are summarized.

2. The Model

We restrict ourselves here to a brief summary of the main features of the numerical modeling. A comprehensive description of the model and computational technique has been given by Gadun et al. (1998a) and the interested reader is referred to that paper. The present numerical code is similar to that used by Atroshchenko & Gadun (1994), Gadun (1995), Gadun & Vorob'yov (1995), Gadun & Pikalov (1996) and Gadun et al. (1997, 1998a,b). The computational domain covers 17.85 Mm in the horizontal direction (510 grid points with a spacing of $\delta x = 35$ km) and 2.03 Mm in the vertical (58 grid points with the same spacing). The temporal step is $\delta t = 0.3$ s and the simulation is run for 301 solar minutes (after an initial relaxation period of 24 min). A total of 602 models separated by 30 s each have been stored and analyzed.

The *system of hydrodynamic equations* is written in conservative form and describes a compressible, radiatively coupled and gravitationally stratified medium under solar conditions. The equation of energy conservation includes radiative heating and cooling, effects of molecular viscosity and of the viscosity described by the Reynolds stress tensor (with contributions from the velocity stress tensor and sub-grid turbulence). The equation of state is given by the ideal gas law. The ionization equilibrium of 15 elements is taken into account in LTE and the influence of H_2 and H_2^+ is included for temperature below 6000 K.

The *solution of the hydrodynamic equations* uses the method of large particles (Belocerkovskij & Davydov 1982) which is derived from the particle-in-cell method (see Amsden 1966 for a review). In order to quantify energy changes due to *radiative cooling and heating* the equation of radiative transfer must be solved. This is done in LTE with the method of moments (i.e. all radiative quantities are averaged over solid angles) using variable Eddington factors. The transfer equation is solved in 97 frequency intervals with the opacity distribution functions of Kurucz (1979) being employed to describe the wavelength dependence. To save computing time the diffusion approximation is used in optically thick layers (photon mean free path below 0.1 km). Periodic *boundary conditions* are imposed on the sides of the computational domain. The top and bottom boundaries are basically open. In addition to the condition that $\partial \mathbf{v}/\partial z$ vanishes at the lower and upper boundary, the average of the internal energy and density is kept constant at the mean value imposed on the very first input model.

The complete data set may now be described by $Q(\mathcal{T}, x, z)$, where $\mathcal{T}$, x and z describe solar time, horizontal position and height, respectively, while Q stands for any physical quantity (such as temperature, horizontal velocity, etc.). We often investigate this data set at a constant height, z_0. In atmospheric layers images of $Q(\mathcal{T}, x, z_0)$ are strongly perturbed or even dominated by p-mode oscillations and waves. They can be identified by their location in the frequency–wavenumber (ω–k) plane in the spatio-temporal Fourier transform $\hat{Q}(\omega, k, z_0)$. Using the method of Title et al. (1986) we applied a spatio-temporal Fourier filter to remove most of the power in the strong 5 and 3 min oscillations. For details we refer to Ploner et al. (1998). Some oscillatory power remains, due mainly to high frequency propagating waves. This cannot be suppressed without unduly influencing the granular pattern. Also, at greater heights the rel-

ative power in the oscillations increases relative to that in the granulation, in accordance with observations (e.g. Deubner et al. 1990). Hence we limit our investigation to $z \leq -26$ km (which is slightly below unit average optical depth at 5000 Å).

3. Simulated granules: fragmenting and dissolving granules

3.1. General Description

Fig. 1a shows the emergent continuum intensity I calculated for $\lambda = 5000$ Å. In this and the following images in Figs. 1 and 2 the x–direction corresponds to the horizontal coordinate of the simulations and the y–direction corresponds to solar time. The intensity image shows a distinct pattern consisting of dark intergranular lanes and bright granules embraced by the lanes. The dark lanes are connected in the sense that a lane once formed does not generally end at a later time, except by merging with another lane. The image hence shows a clear sense of time. A few interruptions can, however, be identified (e.g. at $\mathcal{T} = 2$ h $10'$, $x = 14$ Mm). All such gaps appear to be artifacts introduced by the Fourier filtering since no gaps are present at those times and locations in the original unfiltered image.

The start of a new lane within a bright region and the merging of two lanes are events of particular relevance for our analysis, since they are the clearest signs of granule death and in the former case also of granule birth. This offers a classification of granules into two sets according to the signature and mechanism of its death. One set is characterized by the formation of a new lane within the granule. The "old" or parent granule splits into two "new" granules (children) and the parent is usually called a *fragmenting* granule[1] (e.g. Muller 1989, Title et al. 1989). The other type of granule disappears when the lanes enclosing it merge together, and is called a *dissolving* granule (Mehltretter 1978, Muller 1989). The disappearance of a lane at a given time *may* possibly constitute a third type of granule death, namely the merging of two granules. Such merging granules have been reported on the basis of observations (Mehltretter 1978, Dialetis 1986). In our simulations such cases are very rare and short lived (13 cases out of a total of 462; see Table 1). Due to the poor statistics and because no gaps are present before the Fourier filtering this class has not been studied separately.

The previously given classification of granules by their mode to death implies that granules are only born by fragmentation, whereas observations suggest that some granules grow out of bright points in lanes (Dialetis 1986). We find such splitting lanes in only 5 cases, all of which remain small and vanish within 3 min. This small number may be peculiar to two dimensions.

Figs. 1b to d display the space-time images of the temperature T, pressure p and density ϱ, respectively, all sampled at a fixed height $z = -131$ km ($z = 0$ corresponds to the average height with $\tau = 1$, $\langle z(\tau = 1)\rangle$). The grey scale is chosen such that larger values are brighter. This layer was chosen, since it shows the granular pattern most clearly. Note that $z(\tau = 1)$ is a function of time and space. As a consequence, in layers significantly above $z = -131$ km parts of the image already show a different pattern from granulation, partly reflecting the importance of wave and oscillatory phenomena in layers above the surface.

The temperature in Fig. 1b shows basically the same pattern as the intensity. The intergranular lanes in T, however, are very thin compared to the lanes in I. This is partly caused by the height difference to the surface layer, since at higher z the lanes get somewhat broader, and by the fact that I samples different heights, i.e. bright parts are formed higher whereas dark parts lower in the atmosphere. Consequently, T and I images are expected to be similar but not identical. Also note the dark "dots" often associated with freshly formed lanes in the T-image.

The pressure image in Fig. 1c, in contrast, shows the granulation rather indistinctly, although a careful inspection reveals many, but not all intergranular lanes as areas of enhanced pressure. The regions of large pressure deficit and those of pressure excess often lie close together and are correlated with the lanes. As discussed later, one does not expect the pressure pattern to match for example the granulation pattern reflected in the intensity since pressure excesses are expected both in the interiors of granules (acceleration of horizontal flows) and at their boundaries (downward deflection of the horizontal flow). Another reason for the low correlation between granules and pressure is that the influence of oscillations relative to granulation is largest in the pressure, so that the influence of high frequency waves is also largest in this quantity. Finally, Fig. 1d displays the density, which reflects a pattern, very similar to the temperature (it appears like a negative of Fig. 1b).

3.2. Temporal and spatial boundaries of granules

One aim of the current investigation is to find signatures that are common to many granules and to distinguish these from properties specific to individual granules. This can only be done in a statistical sense. In a first step, we need to identify single granules, i.e we must define the boundaries and moments of birth and death of each granule.

We adopt here the definition that all downflowing gas resides in *intergranular lanes* and that a *granule* is the upflowing gas between two intergranular lanes. This definition makes use of the vertical velocity v_z displayed (at $z = -131$ km) in Fig. 2a. The basic pattern seen in Fig. 1 is also present in the v_z–image. The identification of the granules using v_z is documented by Fig. 2b. Intergranular lanes ($v_z \leq 0$) are plotted dark grey. Among the granules ($v_z > 0$) we distinguish between dissolving granules (light grey) and fragmenting granules (white). This definition of a granule using the vertical velocity component roots in the underlying theoretical interpretation of a granule as a convection cell. The alternative, more observer oriented, definition that granules are locations above a certain intensity threshold, is, we feel, more arbitrary than ours. Nevertheless, we have also isolated granules by intensity and did not find them to deviate significantly from granules defined via v_z for reasonable choices of the intensity threshold, although the isolation of individual

[1] In the present analysis we do not distinguish between exploding granules and other fragmenting granules.

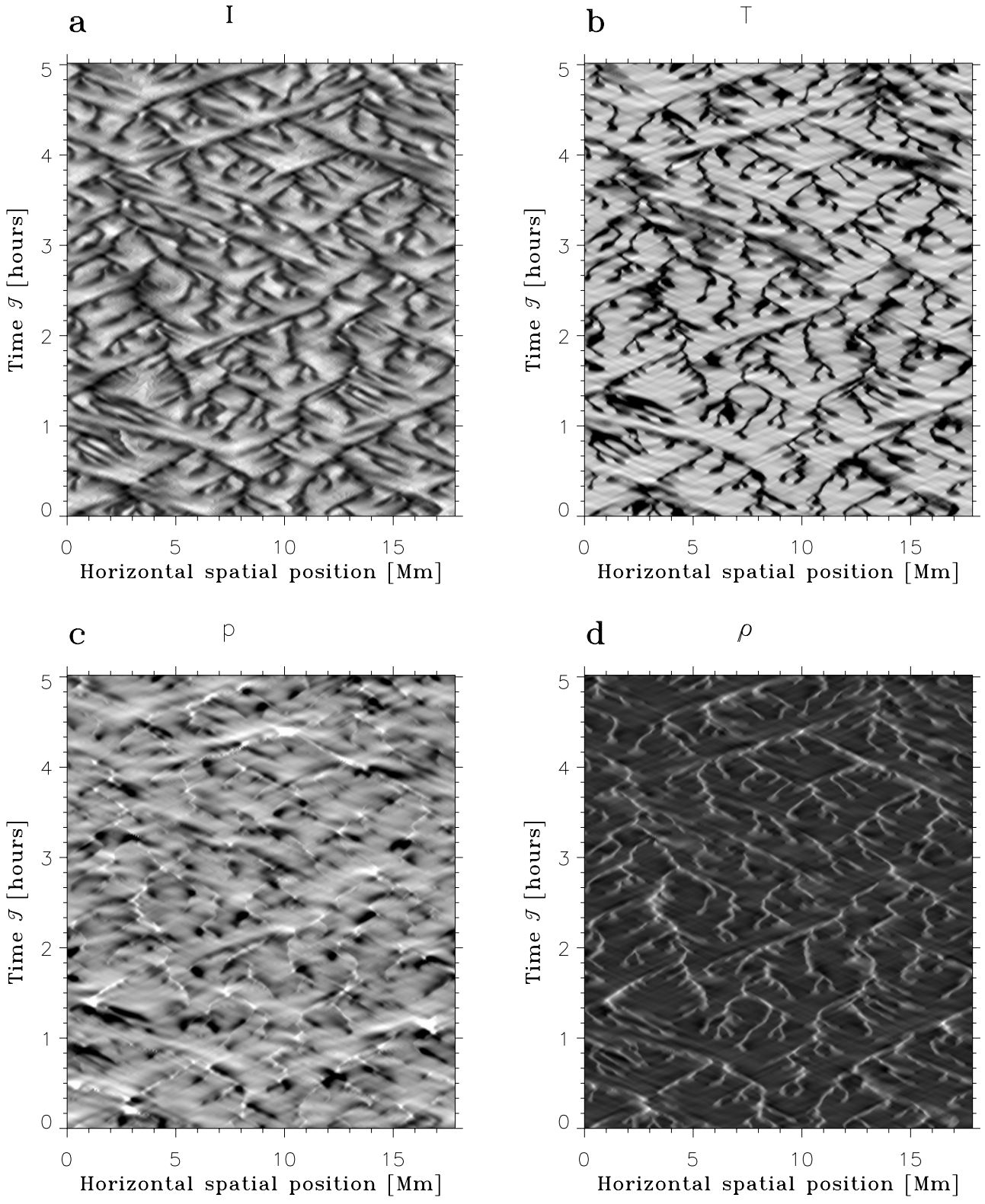

Fig. 1. Frame a: emergent continuum at $\lambda = 5000$ Å as a function of position on the solar surface (i.e. along the computational box) and time. **Frames b** to **d** display the evolution of the temperature, pressure and density, respectively, along horizontal sections through the computational domain. The three physical quantities are displayed for a fixed height $z = -131$ km. The level $z = 0$ corresponds to the average height of continuum formation, $\langle z(\tau = 1)\rangle$. The grey scale for all frames is such, that brighter corresponds to larger values.

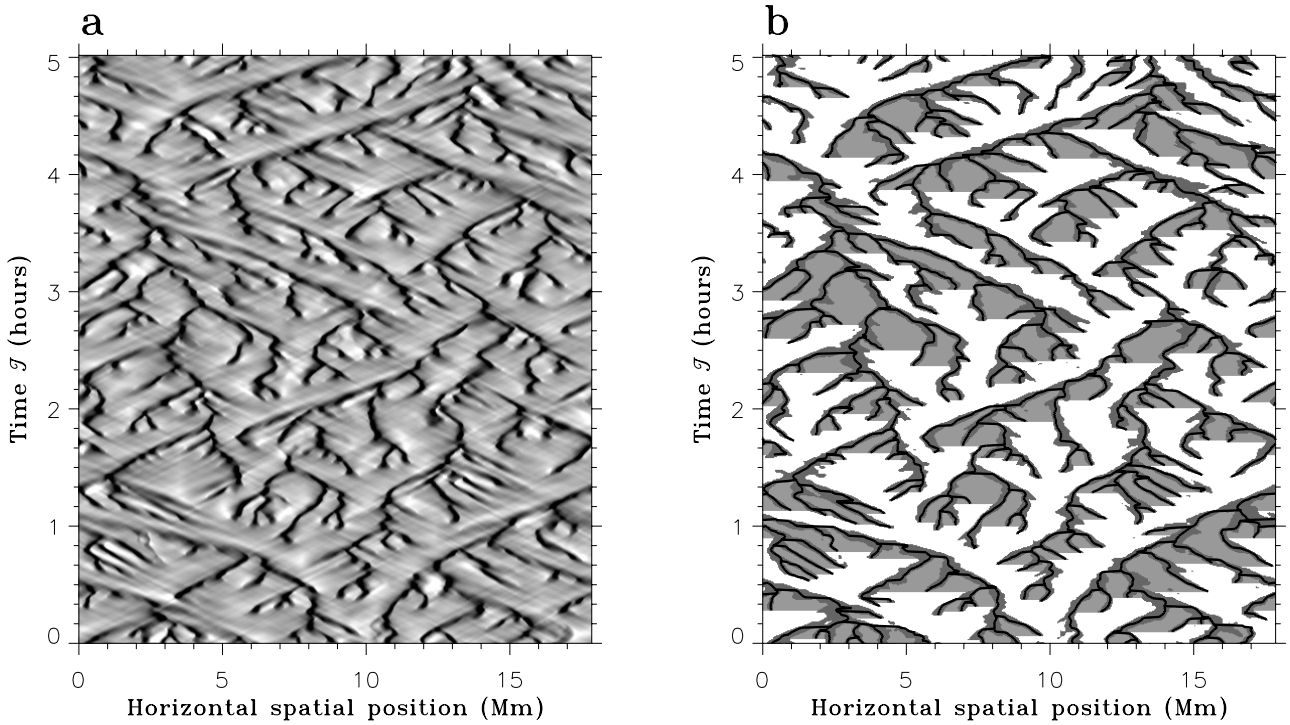

Fig. 2. Frame a: the same as Fig. 1b but now for the vertical velocity. **Frame b**: skeleton of the downflow lanes and of granules. The granule boundaries are marked by the *skeleton* (black solid lines) which corresponds to locations of maximum downflow. The dark grey shaded areas mark downflows ($v_z < 0$), i.e. *intergranular lanes*. The upflows ($v_z > 0$) are separated according to the form of granule death into *fragmenting granules* (white areas) and *dissolving granules* (light grey areas).

Table 1. Number of granules before and after various corrections

	#Di		#Fr		Total
no correction	231		231		462
$\tau \geq 2$ min	218	(-13)	199	(-32)	417

granules by intensity is more cumbersome. The boundaries between granules and lanes found by v_z are later used to extract other physical quantities, e.g. temperature, T, and density, ϱ, for granules and lanes separately.

The spatial boundary between two neighbouring granules (including parts of the intergranular lanes) is given by the "skeleton" of the downflows. Points of the skeleton coincide with the maximum downflow within each lane at each point in time and are displayed by the black lines in Fig. 2b. Fig. 3 illustrates typical evolutions of two granules and may be considered to be the magnification of a typical portion of Fig. 2b. The birth of a granule is best identified by the start of a new intergranular lane (at solar times $\mathcal{T}_1$ and $\mathcal{T}_3$ in Fig. 3). At least in our simulations granules are always born through the fragmentation of their parent granule (neglecting now the few candidates for formation through the merging of new granules or through splitting lanes). The death of a fragmenting granule is marked by the start of a new lane (at $\mathcal{T}_1$ and $\mathcal{T}_3$) whereas the death of a dissolving granule coincides with the merging of two lanes ($\mathcal{T}_2$). According to our definition a dissolving granule dies when no upflow is present anymore. Hence the time of death of the dissolving granule usually does not coincide with the time at which two lanes merge in the skeleton. We often describe the granular evolution by the normalized time, t, which is determined individually for each granule and runs from $t = 0$ at the time of birth to $t = 1$ at its time of death (see Fig. 3).

Due to the finite temporal resolution and the applied Fourier filtering several corrections of the raw skeleton are necessary. As mentioned in Sect. 3.1 a few temporal gaps of the lanes occur which are also present in the wave-filtered v_z-image. None of these gaps is present in the original (unfiltered) image, however, indicating that the gaps are artifacts of the wave-cleaning process. Consequently, the lanes have been connected across the gaps following the uncorrected velocity image. Also, we restricted the lowest lifetime of a granule to be 2 min (4 grid points) for further analysis. This minimum resolution is somewhat arbitrary but considerably facilitates our subsequent analysis. Obviously, such a lower lifetime boundary affects the number of identified granules, as documented by the decrease of the number of granules in the second line of Table 1 relative to those prior to this correction (first line). The number in brackets signify the number of granules affected by this correction.

Another problem has to do with the possibility of single and multiple fragmentation of a granule. Suppose that a granule dies by fragmentation. Suppose further that one of the resulting children itself fragments a short while later. The question then arises whether this second fragmentation is to be attributed to a second (possibly very short-lived) granule, or if it is instead

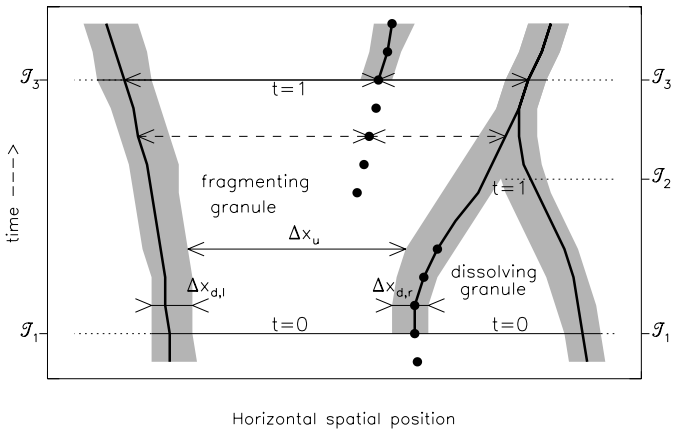

Fig. 3. Illustration of spatial averaging and temporal normalization. The thick solid lines drawn from top to bottom symbolize the skeleton and the shaded areas the corresponding downflows. The dissolving granule on the right is born at time $\mathcal{T}_1$ and lives until $\mathcal{T}_2$, the fragmenting granule lives between $\mathcal{T}_1$ and $\mathcal{T}_3$. The temporal scale is normalized separately for each granule to its lifetime, with $t = 0$ corresponding to the time of birth, and $t = 1$ to the time of death. Spatial averages are formed separately at a fixed time over the upflowing region (indicated by Δx_u for the fragmenting granule) and downflowing region ($\Delta x_{d,l}$ and $\Delta x_{d,r}$, indicated at a different time). The thick dots mark an extrapolation to earlier times of the new lanes formed by granule fragmentation. See the text for more details.

Table 2. Granule statistics

type		Di	Fr	Di+Fr
lifetime	$\langle\tau_g\rangle$	8.55 ± 5.60	7.86 ± 5.75	8.22 ± 5.67
(min)	$1/e$	8.71	6.12	7.33
size	$\langle s\rangle_u$	0.48 ± 0.25	1.70 ± 0.55	1.06 ± 0.74
(Mm)	$\langle s\rangle_d$	0.81 ± 0.23	0.99 ± 0.27	0.90 ± 0.26

better to say that the original granule underwent multiple fragmentation. For these cases our restriction to lifetimes larger than 2 min may be interpreted as saying that successive fragmentations lying 1.5 min or less apart are to be attributed to the same multiply fragmenting granule.

The number of granules is the same at the end and the beginning of the simulation. Since fragmentation increases the number of granules by one (counting each step of fragmentation separately) and dissolution removes one, it is obvious that there must be the same number of fragmenting and dissolving granules in the simulation. The difference in the number of dissolving and fragmenting granules in the second row of Table 1 is therefore an indication of the number of multiple fragmentations. We mention that a similar conservation of the number of granules must hold also in 3–D because the average size of granules and hence their sum does not depend on time (neglecting variations due to solar activity and solar evolution).

Interestingly, the simulation of Wöhl & Nordlund (1985) showed 15% fragmenting, 79% dissolving and 6% merging granules. In their simulation merging granules are the least frequent mode to death suggesting that their rarity in our simulations is not entirely because of the restriction to two spatial dimensions. The reason for their large relative number of dissolving granules remains unclear since they do not give details about their granule classification.

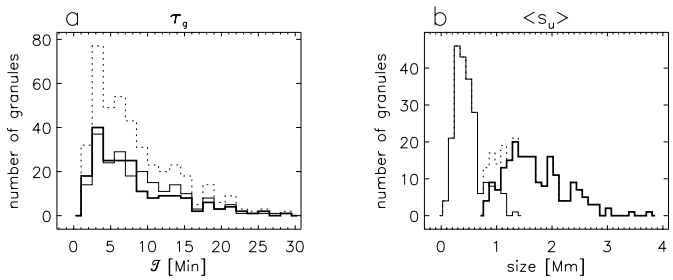

Fig. 4a and b. Histogram of the number of granules versus lifetime, τ_g (**frame a**), and average size of the upflowing region, s_u (**frame b**). Thick solid lines mark the number of fragmenting granules and thin sold lines the number of dissolving granules. The dotted lines display the distributions of all granules. Note that only granules with lifetimes longer than 1.5 min are included.

3.3. Basic statistics

In Table 2 we list the average and $1/e$ lifetime of dissolving, fragmenting and all granules. The $1/e$ lifetime is the time after which only the fraction $1/e$ survives. Also listed are the average sizes of the upflows, $\langle s\rangle_u$, and downflows, $\langle s\rangle_d$. These are averaged over s_u and s_d values of all granules of a certain type at all times (the definitions of s_u and s_d are illustrated in Fig. 3).[2]

According to Table 2 the mean lifetime is lower for fragmenting granules. This is mostly due to rapid successive fragmentation, which gives rise to very short-lived granules (between 2 such splittings). From observations Mehltretter (1978) derives 16 min for the average lifetime of a granule, while Dialetis et al. (1986) obtains 12 min. Finally, Title et al. (1989) find $1/e$ lifetimes in the range of 5 min from SOUP data (degradation of the spatial resolution increases this lifetime up to 10 min). The numbers obtained from our simulations lie between the results of Title et al. (1989) and Dialetis et al. (1986), but are closer to the former. If we keep in mind that the values derived by Title et al. (1989) correspond to larger granules, which live less long, and the fact that we have not counted the shorted-lived granules (Sect. 3.2), then the agreement with their result is expected to be even better.

Fig. 4 shows histograms of the fraction of granules possessing a given lifetime, τ_g (Fig. 4a), and a given average size, s_u (size of the upflow region, Fig. 4b). All in all, the two granule types show very similar lifetime distributions. Together with the fact that both types have the same number of granules the agreement in lifetime distribution indicates that the evolution of dissolving and fragmenting granules is closely related to each other. In the following sections we present strong evidence supporting this hypothesis.

[2] Note the difference to Ploner et al. (1998), who estimated intergranular distances.

The difference in size between the two types of granules is clear from Fig. 4b. The peak of the size distribution of fragmenting granules lies at three times the size of that of dissolving granules and the distribution of sizes of fragmenters is also three times as broad as that of dissolving granules. Between the peaks of the distributions lies a small region of coexistence of fragmenting and dissolving granules. The significantly smaller size of dissolvers compared to fragmenters probably explains why they have been far less studied. The plotted sizes are averaged over the granule lifetimes.

4. Granule evolution

In the previous sections we described qualitatively the occurrence of two types of granules according to the mode of their death. In this section we investigate their evolution in detail and attempt to uncover the physical processes driving it. We begin by considering selected examples each of the evolution of the two types of granules.

4.1. Examples of dissolving and fragmenting granules

In Fig. 5 we discuss, as an example, the profiles of the vertical and horizontal velocity, v_z and v_x, and ϱ, p and T (from top to bottom, respectively) of a dissolving (frame a) and two fragmenting granules (frames b and c). The snapshots are taken at $t = 0.3$ (solid lines) and shortly before death at $t = 1.0$ (dotted line), where normalized time units have been used for t (see Fig. 3 and Sect. 4.2). The granules, defined as upflow regions, lie between the thick dots. Note the different scales on the horizontal axes of Figs. 5a to c, which indicate the difference in size between the three granules.

The dissolving granule viewed at time 0.3 is easily recognizable in all quantities. In addition to the clear up- and downflows seen in v_z it clearly exhibits the signature of an outflow from the centre of the granule in v_x. A low ϱ and relatively high p and T are found in the granule. Note that a pressure maximum in the granule centre and the centre of both lanes is present. The former stops upflowing material and accelerates it to the lateral boundaries of the granules, whereas the latter pushes the horizontally flowing gas downwards along the lanes. By the time of its death ($t = 1.0$) v_z has decreased significantly, the region with $v_z > 0$ has shrunk dramatically and ϱ has increased. The granule is hardly recognizable anymore in v_x, T and p. In particular, the horizontal outflow within the granule has now disappeared and the intergranular lanes on both sides of the dying granule are being fed dominantly by the neighbouring granules (as can be seen from v_z and v_x).

The fragmenting granule in Fig. 5b exhibits an almost opposite temporal evolution, i.e. it expands and more than doubles its size between $t = 0.3$ and $t = 1.0$. As we shall see the large initial pressure drives the expansion. Note the large central pressure excess relative to the dissolving granule (Fig. 5a). Interestingly, as the granule expands and v_x increases in time v_z decreases. At $t = 1.0$, two locations of beginning fragmentation are seen at 14.4 and 15.5 Mm where v_z is about to change sign. The one at 15.5 Mm also reveals a local p and ϱ excess.

Note, that in this example v_z is not largest at the granule boundaries at $t = 1$ and thus does not reflect the behaviour described by Rast (1995) based on a idealized numerical experiment. However, examples agreeing with the findings of Rast are also present in our data set, one of which is given in Fig. 5c. A count indicates that in approximately 30 % of the fragmenting granules v_x exhibits a strong maximum close to the downflow at least at one side of the granule. In approximately 50% no such behaviour could be recognized, while it was not possible to attribute the remaining 20% to either class.

We emphasize that the examples shown in Fig. 5 are selected to reflect the more well-behaved granules. Some granules move horizontally as a whole while others possess a highly distorted horizontal structure such as a v_x that is entirely positive or negative (after subtracting the shift of the whole granule).

4.2. Extraction of the temporal evolution of a mean granule

Due to the comparatively long simulation time and the sufficient horizontal extent of the computational domain the complete evolution of over 400 granules can be followed. Consequently, by averaging over granules at a particular stage of their evolution it is possible to extract the evolution of a typical or mean granule, uncontaminated by the fluctuations due to the details of the history and environment of a particular granule. In order to extract the mean granular evolution the following steps are carried out:

1. The *spatial average* of the physical quantity under consideration is taken at a fixed time for each granule. Averages over the upflowing gas (i.e. over the region marked by Δx_u in the case of the fragmenting granule in Fig. 3) and over the downflow lanes which enclose the considered granule (marked by $\Delta x_{d,l}$ and $\Delta x_{d,r}$) are calculated separately.
2. The (solar) time $\mathcal{T}$ is *normalized* by the lifetime τ_g of the studied granule. Hence birth corresponds to $t = 0$ and death to $t = 1$ (cf. Fig. 3).[3] Then, the physical quantities are interpolated onto a new grid of a total of 100 time steps covering the interval between 0 and 1.
3. The spatially averaged parameters at a given normalized time t are *averaged over all granules* belonging to the same species and separately over the corresponding intergranular lanes.

Strictly speaking the resulting evolutionary profile must be called the spatially averaged, temporally normalized mean granular evolution profile, but we refer to it simply as the *granular evolution profile* or even as *granular evolution*.

In order to detect changes in physical quantities directly associated with the formation of new lanes (such as the two lanes starting at times $\mathcal{T}_1$ and $\mathcal{T}_3$ in Fig. 3), but happening prior to their

[3] The time of death, $t = 1$, corresponds to the first time step at which no upflow is present anymore. For simplicity we identify the last time step, where an upflow is present, with death. Strictly speaking, the granules dies somewhat later.

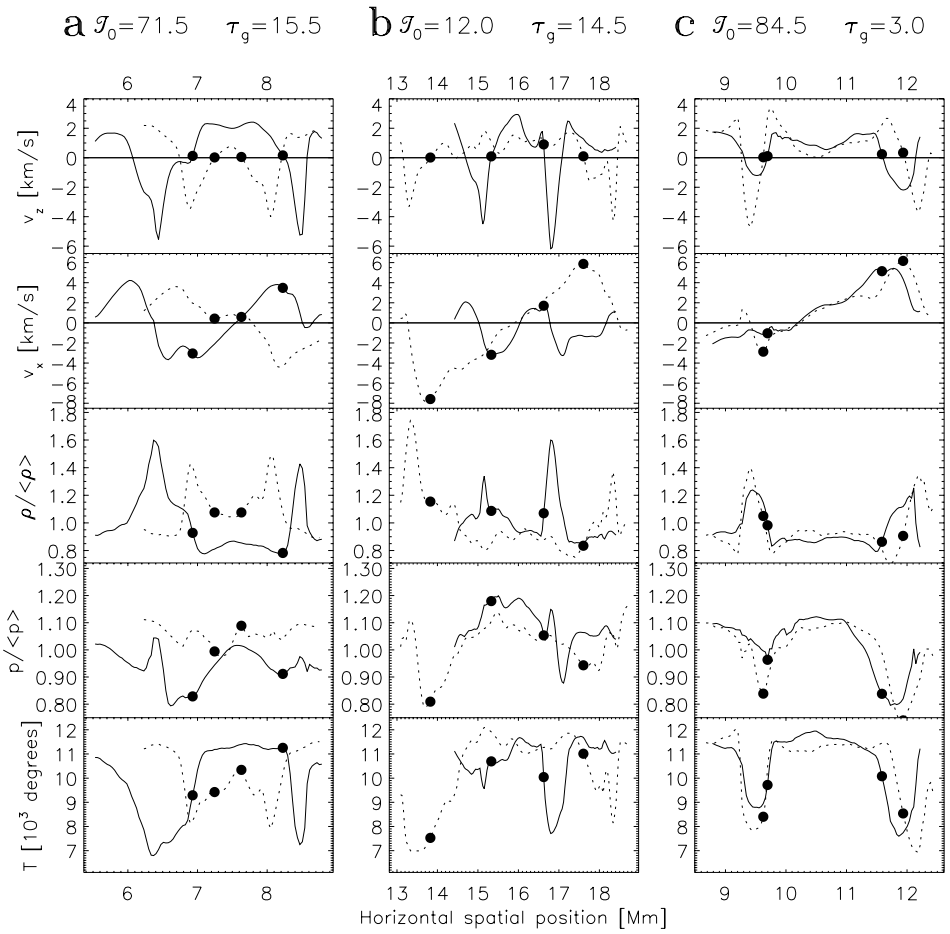

Fig. 5a–c. An example each of the horizontal structure at $z = -131$ km of a dissolving (frame **a**) and two fragmenting granules (frames **b** and **c**). Displayed are from top to bottom the vertical, v_z, and horizontal, v_x, velocity, the density, ϱ, pressure, p, and temperature, T. Solid curves correspond to $t = 0.3$, dotted lines to $t = 1.0$ ($t = 0$ marks the birth and $t = 1$ the death of each granule). Bullets mark the boundaries of the considered granules, i.e. they enclose the upflow ($v_z > 0$). All curves are extended horizontally up to the middle of the two adjacent granules. The absolute values of time of birth, $\mathcal{T}$, and the granule's lifetime, τ_g, are given at the top of each frame in minutes.

birth, the lanes have been extended backward in time for half of the fragmenting granule's lifetime (marked by the thick dots in Fig. 3). In normalized time units the extension corresponds to time 0.5 to 1.0 of the fragmenting granule. The horizontal location of the extension is prescribed by keeping the ratio of the distance to the two neighbouring downflow lanes constant over the whole extension (indicated by the double arrows at death $\mathcal{T}_3$ and two time steps earlier). The data in the freshly born lane is followed up to $t = 1.2$ beyond death. To obtain the mean evolution along these extended lanes we follow No. 2 and 3 of the points listed above. Instead of averaging according to point 1, we take the data along the extended lanes. We refer to this normalized mean evolution along an extended lane in short by the *evolution along a pre-lane*.

4.3. Evolution of fragmenting granules

Fig. 6 displays the granular evolution of T (frame a), normalized p (frame b), normalized ϱ (frame c) and v_z (frame d) of the mean fragmenting granule as defined in Sect. 4.2. From bottom to top the subframes of Figs. 6a to d refer to data taken at height levels $z = -341$, -201, -131 and -26 km, respectively. Consider first the evolution of the upflowing region ($\langle . \rangle_u$, thin solid lines). No significant change is seen either over the lifetime of a granule or over height. For comparison, the corresponding evolution for the averages taken over the adjacent lanes ($\langle . \rangle_d$) are displayed by the dotted curves. Although the changes with time are somewhat larger for the lanes, they are again not significant. This general picture is in agreement with the results reported for large granules by Hirzberger et al. (1997) in the sense that all quantities show significant differences between granules and lanes, with the possible exception of the pressure. Even in the case of the pressure the difference is actually significant, particularly in the highest displayed layer of $z = -26$ km. The plotted error bars are standard deviations and mark the likelihood that any given granule or intergranular lane lies within the plotted error bars. However, the uncertainties of the plotted averages are a factor of roughly $\sqrt{N_{Fr}} \approx 14$ smaller. Hence fragmenting granules have a distinctly larger average pressure than the neighbouring lanes particularly at and above the surface. Note, however, that the maximum pressure in the lane (not shown) is practically the same as in the granule. This agrees completely with the findings of Hurlburt et al. (1984). They find that a (central) pressure excess in the granule accelerates the vertically rising gas sideway to the boundaries where another pressure excess propels the gas downwards.

In agreement with this the expected temporal transition from the characteristics of a granules ($v_z > 0$) to that of a lane ($v_z < 0$) is clearly seen. Since it is caused by a local instability, little sign of the impending fragmentation of the granule is seen in

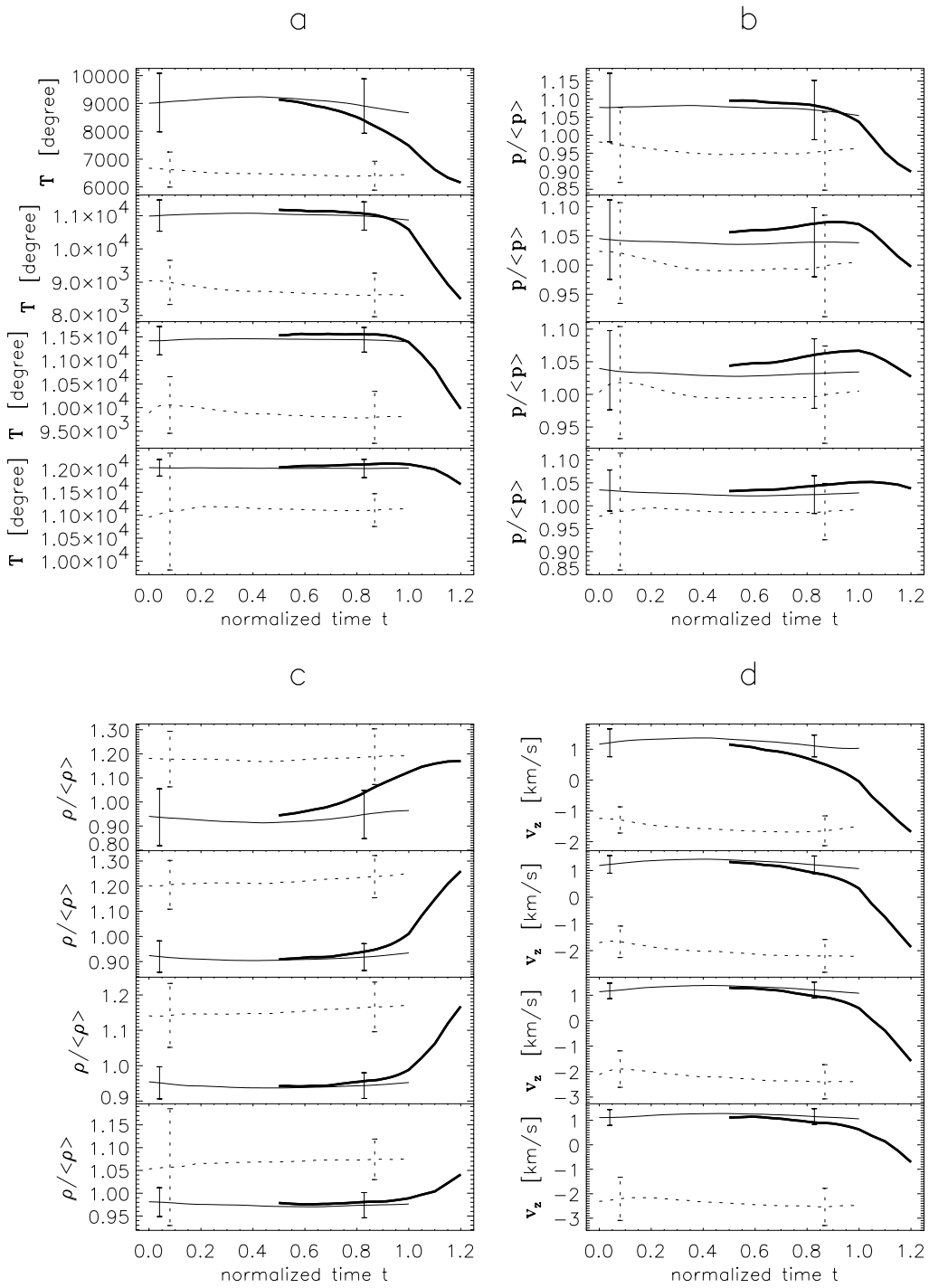

Fig. 6a–d. Evolution of the mean fragmenting granule and associated mean downflows at four heights. The physical quantities are the temperature T (frame **a**), pressure p (frame **b**), density ϱ (frame **c**), and vertical velocity v_z (frame **d**). p and ϱ have been normalized by dividing them by their global averages at the same z. The subframes in **a** to **d** correspond to $z = -341$, -201, -131 and -26 km from bottom to top, respectively. Thin solid lines display the mean evolution of fragmenting granules (denoted by $\langle . \rangle_u$, see the definition in Sect. 4.2), while dotted lines correspond to the mean evolution of the adjacent downflows ($\langle . \rangle_d$). The thick curves show the evolution along the pre-lane and the lane formed through the fragmentation. The error bars indicate the scatter in values from one granule to the next (standard deviation).

these averages. Along the pre-lane (thick lines in Fig. 6), the changes in T, v_z and ϱ first start at the level $z = -26$ km and at increasingly later times with increasing depth. The behaviour of the pressure is interesting. The local pressure in the pre-lanes is already above average at $t = 0.5$. The pressure then increases, most strongly between $z = -201$ and $z = -131$ km, i.e. below the layer $z = -26$ km where T, p and ϱ reveal the largest and earliest variation. At this layer the pressure does not increase at all. Hence, Fig. 6 is telling us that a pressure increase just below the surface is accompanied by a density increase and a temperature and vertical velocity decrease at the surface. The excess pressure begins to slow the rising hot material down. This material manages to overshoot the layers exhibiting the enhanced pressure but only with a greatly reduced v_z. The lower v_z allows the material to cool down (as we shall see in Fig. 7, v_x also decreases with time in the pre-lane), which then leads to the enhanced density and finally to a reduced buoyancy. The evolution of all these quantities is in good agreement with the well known buoyancy-braking mechanism, which leads to the formation of new downflows (Massaguer & Zahn 1980, Latour

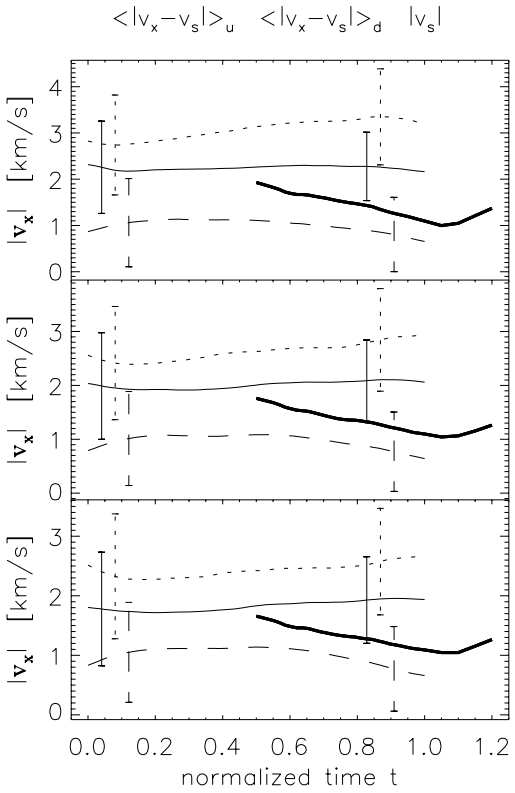

Fig. 7. Evolution of different horizontal velocities. The subframes correspond to $z = -201$, -131 and -26 km from bottom to top, respectively. The thin solid line refers to $\langle|v_x - v_s|\rangle_u$, where v_s is the shift of the whole convection cell. The dotted line displays the evolution of $\langle|v_x - v_s|\rangle_d$, while the evolution of the shift $|v_s|$ is displayed by the dashed line. The thick lines trace the evolution of $|v_x - v_s|$ along the pre-lanes.

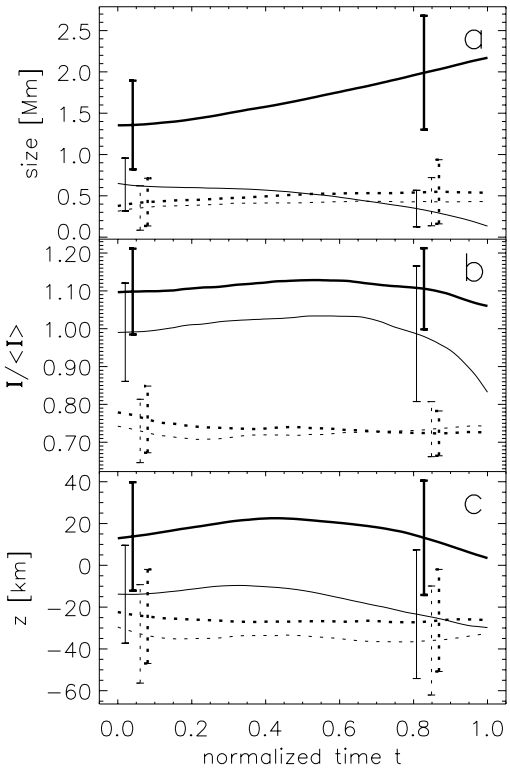

Fig. 8a-c. Evolution of **a** the size, s, **b** continuum intensity, I and **c** height of continuum formation, $z(\tau = 1)$, of dissolving and fragmenting granules. Averages over granules ($\langle . \rangle_u$) are displayed by solid lines, averages over lanes ($\langle . \rangle_d$) by dotted lines. Thick lines: quantities referring to fragmenting granules, thin lines: dissolving granules.

et al. 1983), which has previously been recognized in 3–D (e.g. Nordlund 1985, Steffen et al. 1989) as well as in 2–D simulations (e.g. Freytag et al. 1996). Note that in Fig. 6 T, p, ϱ and v_z in the newly born lanes (thick curves for $t > 1$) overshoot the corresponding average values of the previously existing lanes because only the location of maximum downflows contribute to the thick curves.

The evolution of the horizontal velocity is displayed in Fig. 7 for levels $z = -201$, -131 and -26 km (bottom to top). The thin solid lines represent $\langle|v_x - v_s|\rangle_u$, which is the horizontal velocity corrected for the shift of the whole granule, v_s. The shift v_s is determined from the average motion of the neighbouring intergranular lanes. When determining $\langle|v_x - v_s|\rangle_u$ we first take the absolute value of the difference and only then do we average horizontally over the granule (i.e. upflowing region). This quantity does not show significant change over time although it *un*surprisingly increases with increasing height. The same quantity averaged over downflows, $\langle|v_x - v_s|\rangle_d$ (dotted lines) shows a certain tendency to increase with time. But the most striking feature is that $\langle|v_x - v_s|\rangle_d > \langle|v_x - v_s|\rangle_u$, i.e. the largest horizontal velocities are located at the granule boundary. Along the pre-lanes (thick line) $|v_x - v_s|$ is smaller than $\langle|v_x - v_s|\rangle_u$ and decreases with time until fragmentation. This fits in with the buoyancy braking scenario presented above. After the formation of the new lane $|v_x - v_s|$ starts to increase again, in accordance with the other intergranular lanes.

4.4. Evolution of dissolving granules

The evolution of dissolving granules is best studied in direct comparison with the much better understood fragmenting granules. Frames a to c of Fig. 8 show the evolution of the size, s, intensity, I, and the height $\langle z(\tau = 1)\rangle$ of dissolving granules (thin lines) and fragmenting granules (thick lines). The dissolving granules (thin solid curve in Fig. 8a) are considerably smaller than the fragmenting granules (thick solid curve) already at birth. This discrepancy in size mounts rapidly, clearly illustrating the opposite evolution of the size of fragmenting and dissolving granules. The size of the former increases steadily, almost doubling in the course of their lifetime, whereas the size of the latter decreases until they disappear.[4] In addition to the granules themselves the average size of the adjacent downflows to each type of granule is displayed in Fig. 8a (dotted curves). Obviously, the downflows embracing the fragmenting and dissolving granules are of similar size.

[4] Since the true time of death is shortly after $t = 1$, the size of dissolving granules remains positive (thin solid line in Fig. 8a).

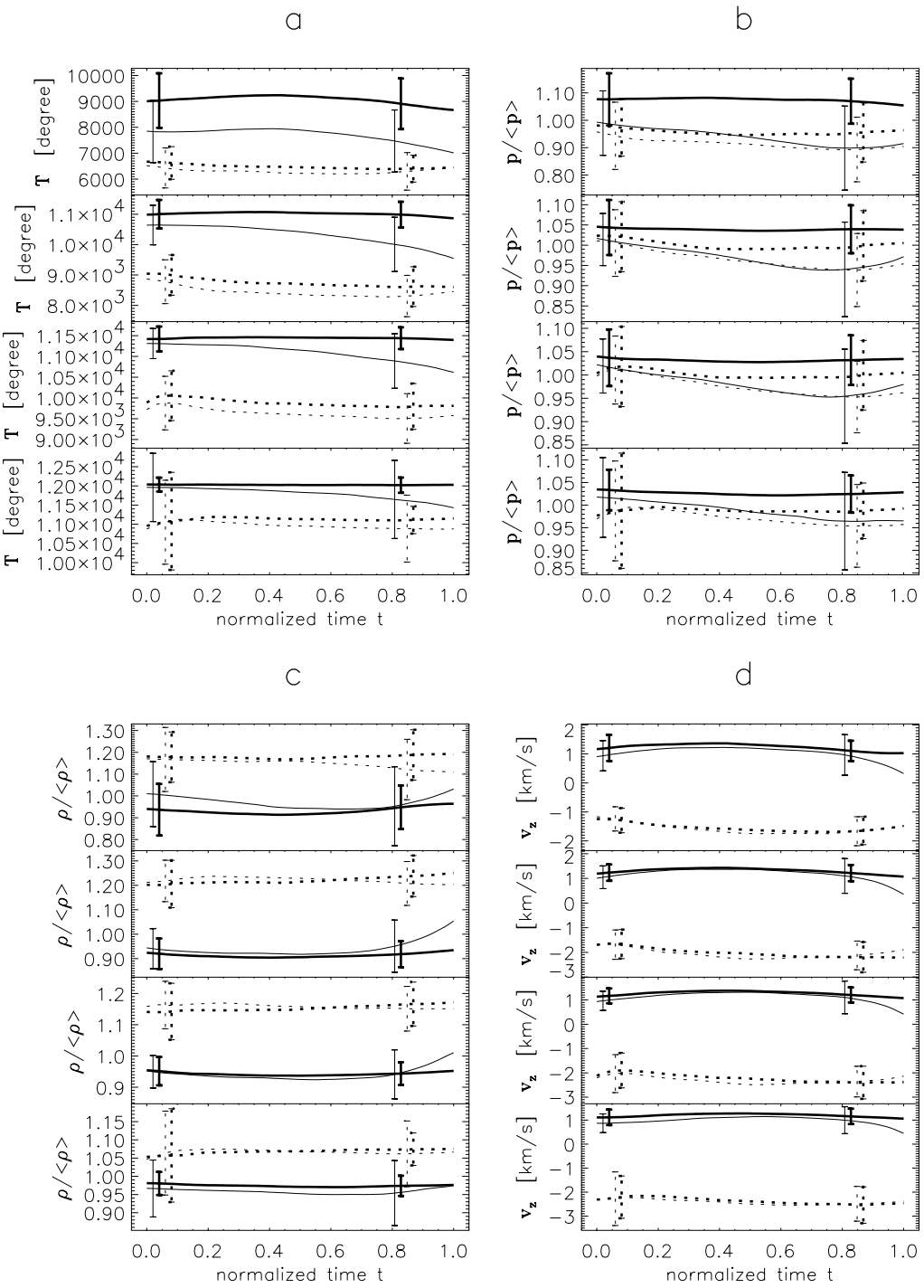

Fig. 9a–d. Evolution of dissolving and fragmenting granules. The same as Fig. 6 but now for dissolving (thin lines) and fragmenting (thick lines) granules and without the evolution along the pre-lane. Averages over granules ($\langle . \rangle_u$) are displayed by solid, averages over lanes ($\langle . \rangle_d$) by dotted lines.

A difference in brightness between fragmenting and dissolving granules is visible in Fig. 8b (solid lines). The lanes (dotted lines) do not differ in brightness between the two types of granules.

Fig. 8c reveals that the visible surface of fragmenting granules lies higher than that of dissolvers. Note that this figure justifies that the chosen uppermost displayed layer is $z = -26$ because at higher layers the granular pattern of dissolvers becomes indistinct.

Fig. 9 compares the evolution of fragmenting (thick lines) and dissolving (thin lines) granules in T, normalized p, normalized ϱ and v_z (frames a to d, respectively). The difference in T (Fig. 9a) between the two types of granules is almost time independent at $z = -26$ km. At greater depth the fragmenting granule shows no change over time while dissolving granules cool significantly. This temperature decrease accelerates as the granules becomes smaller. We expect that this decrease in T, which is most pronounced in the upper layers, could be partly

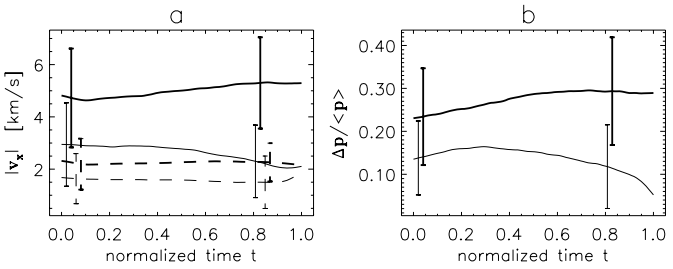

Fig. 10a and b. Evolution of the horizontal velocity and normalized pressure difference of fragmenting (thick lines) and dissolving (thin lines) granules. Frame **a** corresponds to $\max_u(|v_x - v_s|)$ (solid line) and $\langle|v_x - v_s|\rangle_u$ (dashed lines). Frame **b** displays $\Delta\tilde{p} = \max_u(\tilde{p}) - \min_u(\tilde{p})$, i.e. the largest pressure difference within a granule, where $\tilde{p} = p/\langle p\rangle$.

due to radiative cooling. Steffen et al. (1989) demonstrated that small convection cells, such as dissolving granules, radiate very efficiently in the horizontal direction, leading to a drop in temperature.

The average pressure (Fig. 9b) of dissolvers lies below that of fragmenters at all times and decreases right from the start of their evolution. This pressure decrease is partly driven by the enhanced radiative cooling and partly by the decreasing size of the granule (see the discussion on mass conservation below). Note that the average pressure hardly differs between dissolving granules and their neighbouring downflowing lanes. Up to $t \approx 0.7$ the density and vertical velocity (Figs. 9c and d) of the dissolving granules does not deviate significantly from the respective quantities of the fragmenting granules at all considered heights. Shortly before dissolution the physical parameters exhibit a behaviour that is very reminiscent of buoyancy braking: the density and pressure of the dissolver increase and brake the upflow after a short time lag. Note that as in the case of fragmenting granules the final pressure enhancement is not visible in the topmost layer. Note also that the downflow lanes remain practically unchanged.

Although Fig. 9 suggests that the final death of dissolving granules is caused by buoyancy braking, it gives few clues to the mechanisms driving the earlier evolution. As Fig. 8a shows, dissolvers start shrinking soon after birth. Uncovering the cause of this is the aim of Sect. 4.5.

Let us now discuss the horizontal velocities. These are displayed in Fig. 10a. The evolution of $\langle|v_x - v_s|\rangle_u$ (dashed lines) remains constant over time for both fragmenting (thick lines) and dissolving (thin lines) granules. In contrast, $\max_u(|v_x - v_s|)$ (solid lines) decreases for dissolving and increases somewhat for fragmenting granules. Both $\langle|v_x - v_s|\rangle_u$ and $\max_u(|v_x - v_s|)$ exhibit the same evolution at all depths but decrease in magnitude as z decreases. Note that v_x is expected to scale with size s due to mass conservation (e.g., Steffen et al. 1989, Spruit et al. 1990, Schüssler 1992, Stein & Nordlund 1998). It demands that the overshooting mass passing vertically through the area covered by the 2-D granule ($= \varrho v_z(2r)$, where r is the granule radius) must leave the granule through its lateral boundary within a density scale height ($= \varrho v_x(2H)$, where H is the density scale height). As a result the horizontal velocity scales with the granule's size,

$$v_x \sim r. \tag{1}$$

This scaling can only be recognized in maximum horizontal velocity and not in the average velocity. Even in the maximum velocity it is not followed rigorously, since real granules are neither in a steady state, nor do they possess an upflow that is uniform over the granule (see Sect. 4.5.2). v_x is related to the dynamical pressure via $\varrho\, v_x^2$. Consequently, an increase δv_x causes a pressure excess δp which can be expressed using Eq. (1) as

$$\delta p \sim r^2 \tag{2}$$

In Fig. 10b we test this by plotting as a measure for δp the difference between maximum and minimum pressure, $\Delta p = \max_u(p) - \min_u(p)$. The relation between $\max_u(|v_x - v_s|)$ and $\max_u(p)$ is basically in accordance with Eq. (2) for the dissolving granules. Note that this suggests the rapid decrease in pressure of the dissolving granules is at least partially caused by the shrinking size via mass conservation. Fragmenting granules show a more leisurely increase in pressure excess than expected from the velocity.

4.5. Interaction between granules

4.5.1. Relation between granules and their neighbours

In this section we investigate the temporal evolution of granules relative to their neighbours. At each time step, in addition to the granule under consideration, the adjacent halves of the neighbouring granules are also studied. The averages of the physical quantities over these halves are computed and subtracted from the corresponding average of the intervening granule. The temporal evolution of the relative differences of various quantities, formed as described above, is plotted in Fig. 11.

The most remarkable feature of this figure is that whereas fragmenting granules possess a T and p excess relative to their neighbours dissolving granules suffer from a T and p deficit. From birth dissolvers start with a deficit in T and p that is particularly pronounced at the highest plotted level, $z = -26$ km. These deficits further increase with time. Dissolving granules are, however, relatively neutral relative to their neighbours in ϱ and v_z, except towards the ends of their lives, when they obtain a strong ϱ excess and v_z deficit. The time dependence of all differences is much larger for dissolving granules than for fragmenters. Nevertheless, even for the fragmenting granules changes in the differences to neighbours are larger than in the absolute values of the physical quantities.

Fig. 11 emphasizes that the evolution of a granule cannot be separated from that of its surroundings. It is always in competition with its neighbours for more space. The pressure difference between neighbouring granules gives rise to a force pointing from higher to lower pressure, i.e. away from fragmenting and towards dissolving granules. The following comparison of the horizontal velocities indicates the close relation to such pressure

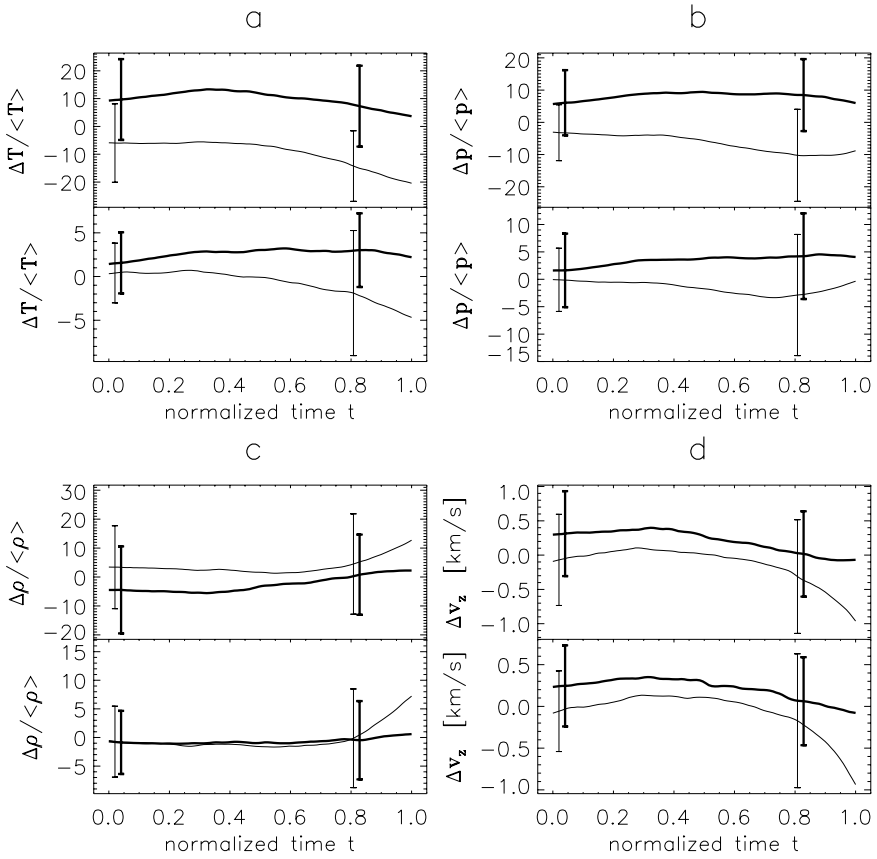

Fig. 11a–d. Properties of granules relative to their neighbours. The percentage of the averages of the normalized difference of temperature $\Delta T/\langle T\rangle$, pressure $\Delta p/\langle p\rangle$, density $\Delta\varrho/\langle\varrho\rangle$ (**a** to **c**, respectively) and the difference in the vertical velocity Δv_z **d** are plotted vs. t. The average of each quantity over half of each of the two adjacent granules is subtracted from the average over the granule in between. Thick lines refer to fragmenting, thin lines to dissolving granules. Bottom and top frames refer to $z = -201$ and -26 km, respectively.

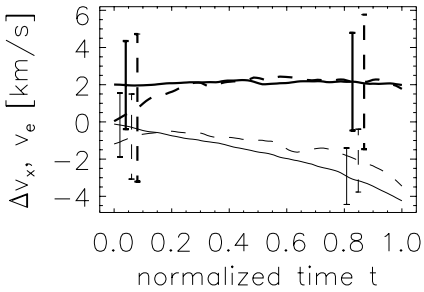

Fig. 12. Difference between the horizontal velocity of granules and their neighbours, Δv_x (solid, see in the text for a definition), and the average rate of change in size of granules $v_e = ds/dt$ (dashed lines). Both quantities are plotted at the level $z = -26$ km versus normalized time t. Fragmenting granules correspond to thick lines, dissolvers to thin lines.

gradients. Let x_{u1} and x_{u2} be the left and right boundaries of the granule (i.e. of the upflowing gas). Let further x_{ul} (x_{ur}) be the closest upflowing point of the adjacent granule on the left (right). Then $2\Delta v_x = \{v_x(x_{u2}) - v_x(x_{ur})\} - \{v_x(x_{u1}) - v_x(x_{ul})\}$ is a measure of whether the outflow in the granule being studied is larger ($\Delta v_x > 0$) or smaller than in its neighbour ($\Delta v_x < 0$). Δv_x is plotted in Fig. 12 for fragmenting (thick solid lines) and dissolving granules (thin solid lines). The fragmenting granules reveal a constant excess outflow. In contrast, the dissolving granules rapidly loose the competition with their stronger neighbours, with their outflows becoming ever weaker relative to those of the adjacent granules. The same qualitative picture is also seen at other heights.

Also plotted in Fig. 12 is the rate of change in granule size, $\partial s/\partial t$, displayed by the dashed lines. The agreement between Δv_x and $\partial s/\partial t$ is remarkable and strongly supports the idea that the rapid outflows are responsible for the rapid expansion of fragmenters. In order to brake these outflows a considerable pressure excess builds up over the surrounding downflows in order to break them. If this pressure is larger than over the neighbouring granule then the lane moves outward, allowing the granule to expand. The opposite effect causes the contraction of dissolvers.

4.5.2. Horizontal structure of granules

In an ideal, symmetric convection cell at rest positive divergence is expected, i.e. plasma flows from the central part of the cell towards its boundary. For such an ideal granule $|\langle v_x - v_s\rangle|$ obviously vanishes whereas $\langle|v_x - v_s|\rangle > 0$. For an extremely asymmetric granule with a purely unidirectional v_x, however, the quantities $|\langle v_x - v_s\rangle|$ and $\langle|v_x - v_s|\rangle_u$ are the same. Note that $|\langle v_x - v_s\rangle| \le \langle|v_x - v_s|\rangle$ must always hold. Fig. 13 shows the temporal evolution of $\langle|v_x - v_s|\rangle$ (solid line) and $|\langle v_x - v_s\rangle|$ (dashed) for fragmenting (thick lines) and dissolving (thin lines) granules. Fragmenting granules start with a highly asymmetric horizontal velocity, i.e. $|\langle v_x - v_s\rangle|$ is on average close to $\langle|v_x - v_s|\rangle$. This is not surprising since new-born granules are

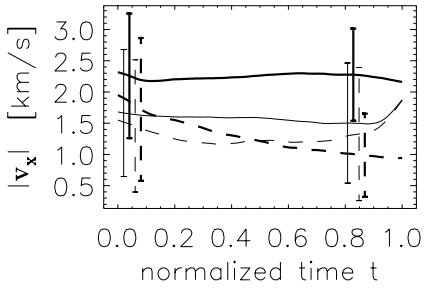

Fig. 13. Absolute horizontal velocity, $\langle|v_x - v_s|\rangle$ (solid lines), and absolute value of the net horizontal velocities, $|\langle v_x - v_s\rangle|$ (dashed lines), averaged over granules at height level $z = -26$ km. A comparison between these quantities provides a measure of the asymmetry of the horizontal velocity flow. Plotted is the height level $z = -26$ km Fragmenting granules correspond to thick lines, dissolvers to thin lines.

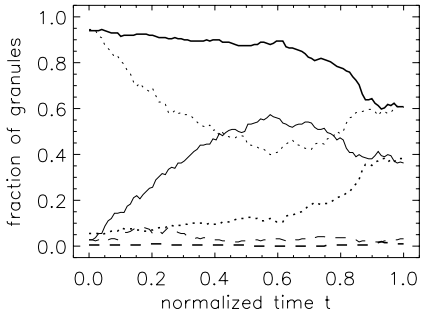

Fig. 14. Fraction of granules with different horizontal flow structures vs. normalized time. The solid lines display the fraction of granules with positive divergence (i.e. $v_x - v_s$ points outwards on both sides of the granules), while dashed curves corresponds to negative divergence. The dotted lines indicate the fraction of granules for which $v_x - v_s$ has only one sign everywhere within the granule, i.e. the horizontal flow is purely unidirectional over the whole granule. Thick curves mark fragmenting and thin dissolving granules.

fragments of the parent granule. During the course of their evolution the cells seem to reorganize themselves and establish a fairly symmetric flow ($|\langle v_x - v_s\rangle|$ decreases, but compare with later). The dissolving granules posses a highly distorted velocity structure not just at birth, but throughout their lifetime. Unlike fragmenters the smaller dissolving granules are not able to build up a strong symmetric flow. Although, initially there is also a tendency for the flow to become more symmetric, $|\langle v_x - v_s\rangle|$ and $\langle|v_x - v_s|\rangle$ are practically equal again shortly before the death of the mean dissolving granule.

In view of the surprising asymmetry of dissolving granules we now check how frequent granules with a completely unidirectional horizontal velocity are, i.e. we check if at a given time a granule possesses positive divergence (i.e., $v_x - v_s$ changes sign within the granule and corresponds to an outflow), negative divergence ($v_x - v_s$ corresponds to an inflow into the granule), or a horizontal flow in one direction ($v_x - v_s$ does not change sign anywhere in the granule; zero divergence). Note that this terminology of "divergence" is not strictly correct since the density has not been taken into account. The fractions of granules with positive divergence (solid curve), negative divergence (dashed curve) and zero divergence (dotted curve) are displayed in Fig. 14 as a function of normalized time. The counts have been normalized such that the sum over all three classes is unity. For both fragmenting and dissolving granules the number of cases of negative divergence is negligible, although a few such dissolvers are present. Most of the fragmenting granules start with positive divergence, but a surprising number lose this property towards the end of their lives. The number of fragmenting granules having a unidirectional horizontal velocity increases correspondingly. This emphasizes that an asymmetry of the convection cell with respect to its centre is built up and one side of the fragmenting granule becomes more powerful than the other. Note the seeming contradiction to Fig. 13 (thick lines) which suggests the opposite evolution in time, namely that on average the velocity structure becomes more symmetric with time. But note that $|\langle v_x - v_s\rangle|$ is dominated by large velocity contributions and does not take into account the sign of the velocity. In particular, a purely unidirectional velocity cannot be distinguished from a granule having one strong and one weak outflow. It fails therefore to reflect the true granular flow structure.

The young dissolving granules have one persisting horizontal velocity in 95% of the cases. This number decreases before the final increase to 60%. One cause of the unidirectional velocity is given by the situation at birth, where the fragment basically inherits the v_x from its parent granule. We investigate next whether the maxima of temperature, upflow velocity and pressure and minimum density are closer to the geometrical centre of a granule or to its edges. To study this statistically a granule is divided into 4 sections of equal horizontal extent at a given height. The granules with maxima, respectively minima of the studied quantity located in either of the two central sections are binned together, as are those with maxima in the two outer sections. The evolution of the fraction of granules with these maxima, respectively minima lying closer to the centre (solid lines) or the edges (dashed) is displayed in Fig. 15.

Let us first consider fragmenting granules. The temperature maximum exhibits no preferred location (thick lines in Fig. 15a) below the surface. At $z = -26$ km, however, the granules appear to reorganize themselves so as to produce a central T maximum. The maximum pressure (Fig. 15b) tends to be more centrally located at both displayed heights, except close to death. The largest upflows (Fig. 15d) preferentially occur near the boundary at birth which is probably a result of the preceding fragmentation of the parent granule. Closer to granule death a central upflow becomes more prominent and dominates in the majority of fragmenters. The remaining 30% of fragmenting granules having maximum upflow closer to a lane indicate the behaviour found by Rast (1995) and agree with the estimate given in Sect. 4.1.

Remarkably, the locations of the corresponding maxima and minima of the dissolving granules (thin lines in Fig. 15) often show the opposite tendency, i.e. maxima or minima lying in the inner part of the fragmenting granules are in most cases found in the outer part of dissolving granules and vice versa. The only exception is the temperature. Note in particular that the pressure

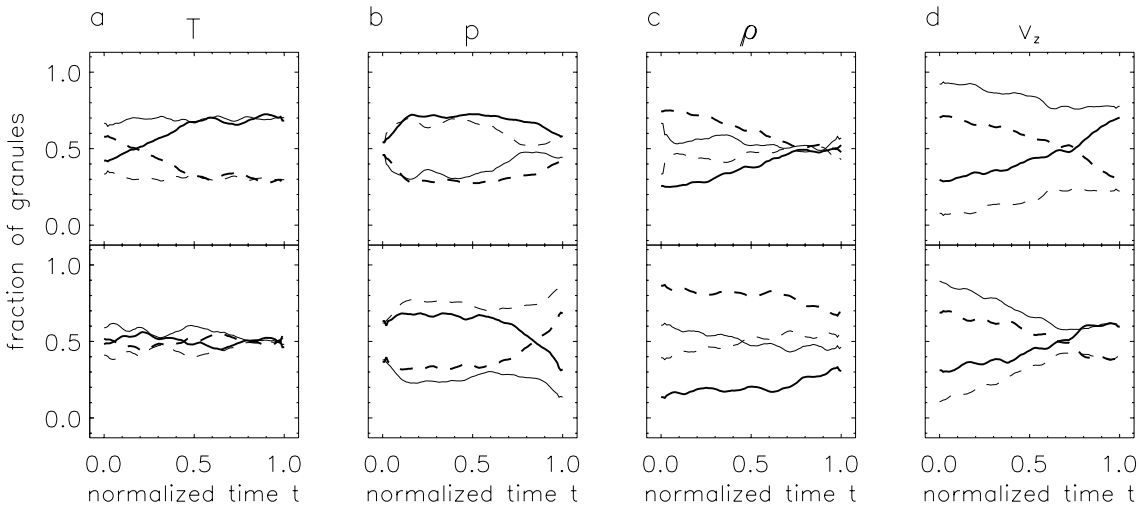

Fig. 15a–d. Fractions of granules with different horizontal structures in four physical quantities are plotted vs. t at height levels $z = -201$ (bottom) and -26 km (top). The fraction of granules in which maximum temperature (frame **a**), maximum pressure (frame **b**), minimum density (frame **c**) and maximum vertical velocity (frame **d**) are reached in the central half of the granule is represented by solid lines, while those with the respective extrema of these quantities near the granule boundaries are indicated by dashed lines. As usual, thick and thin lines distinguish between fragmenters and dissolvers.

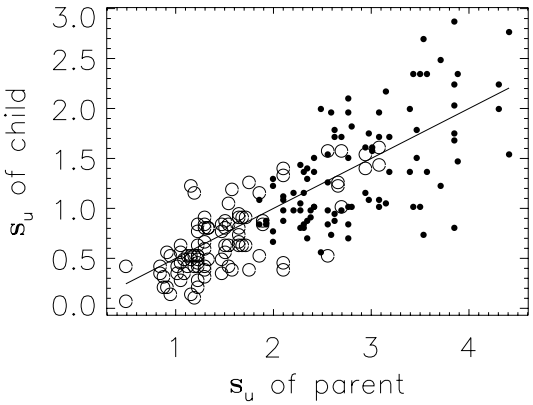

Fig. 16. Scatter plot of the spatially averaged properties of newly born granules (children) vs. the parent granule just prior to fragmentation. Only those fragmenters are shown of which both offspring either dissolve (marked by open circles) or fragment again (marked by dots). Each child is considered separately. Displayed is the granule's size. Points on the solid line mark granules that split into two equal halves.

shows a clear tendency to be largest near the boundary of dissolvers, whereas the largest upflow velocity is rather dominantly located in the central part. In particular the location of the pressure excess near the granule boundary agrees with the finding that a large fraction, even the majority, of dissolvers harbours a unidirectional horizontal flow.

4.6. Granule twins: are they marked for life?

Finally, we consider the question of how decisive the conditions at birth are for the future fate of a newborn granule. The spatial average of the physical quantities (cf. Fig. 8) showed that dissolving granules are cooler, have lower pressure and are much smaller in size than the fragmenting granules already at birth. This difference then increases as the granule evolves.

The birth of a granule (as studied here) is only possible when its parent granule fragments. We now compare the situation before fragmentation with the properties of the fragments in order to learn if parents pass on some of their traits to their children and how strongly the situation at birth (so to say the genetic material) of each of the two granule twins decides their evolution. We only consider the cases when two fragments are formed, so that all granules analyzed in the following are born as twins.

Fragmenting granules can be classified according to the types of their children. The three possible groups consist of

(1) those fragmenting granules both of whose children dissolve: Fr→(Di,Di). Approximately 25% of the fragmenting granules are of this type;
(2) both children fragment: Fr→(Fr,Fr), also approximately 25% of fragmenters;
(3) of fragmenting granules of which one offspring dissolves while the other fragments: Fr→(Di,Fr).Roughly 50% of the fragmenting granules.

Figs. 16 and 17 shows scatter plots of physical parameters of both children of a granule just after birth (y-axis) versus the same parameters of the parent granule just before fragmentation (x-axis). Consequently, for each fragmenting granule on the x-axis two corresponding entries on the y-axis are found. Fig. 16 shows the two families in which both fragments either dissolve (marked by open circles) or fragment again (marked by dots), Fig. 17 shows those cases when one of the offspring dissolves and the other fragments. Points on the solid line in frame a of Figs. 16 and 17a correspond to granules which split into two equal halves. Points on the solid line in the remaining frames

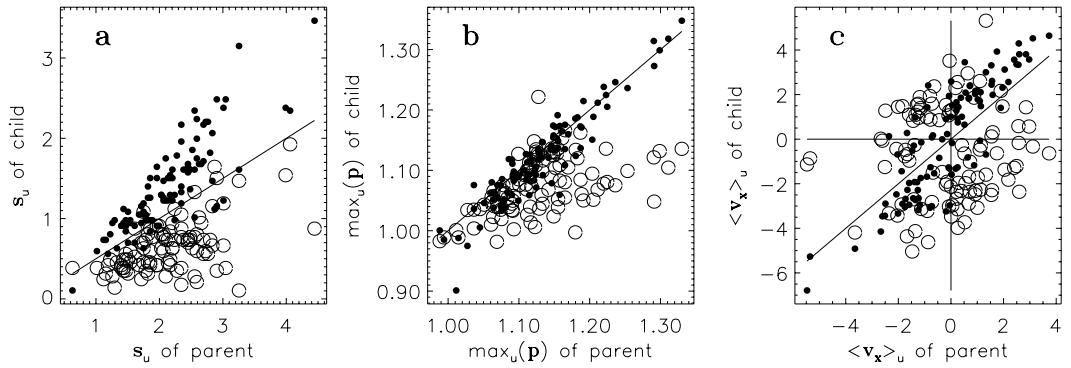

Fig. 17a–c. Frame a shows the same as Fig. 16a, but now for those fragmenting granules of which one offspring dissolves and (marked by open circles) and one fragments marked by open dotted). Frame **b** shows the maximum pressure and frame **c** v_x.

correspond to cases in which the average of the parameter under consideration is the same before and after fragmentation.

The comparison between the granule size before and after fragmentation (Fig. 16) shows that larger granules (size above 3 Mm) tend to split into granules which fragment again. If the parent is less than $\approx$ 2 Mm across, however, at least one of the offspring will dissolve (compare also with Figs. 17a). There is considerable overlap between the thermodynamic quantities (not shown) of the two families, although those with fragmenting offspring tend to have somewhat higher temperature and lower density.

Properties of the remaining fragmenters and their offspring, of which one dissolves and one fragments, are compared in Fig. 17. This family is particularly interesting because it promises the clearest signs of those differences at birth, which could lead to the different subsequent evolutions of the offspring. The comparison of the sizes of the newborn twins clearly shows that with very few exceptions the larger of these fragments again fragments whereas the smaller one dissolves. Obviously, the subsequent evolution is characterized by intense sibling rivalry, with the larger of these winning. It generates larger horizontal flows, which in turn can only be produced by larger pressure, which pushes the smaller sibling away or forces it to contract. Fragmenting and dissolving siblings have otherwise similar physical parameters, including the thermodynamic quantities, with the exception of maximum pressure (Fig. 17b). Fragmenting children possess higher pressure on average. Compare now the $\langle v_x \rangle_u$ of the parent with that of the child (Fig. 17c). The children with the same sign of $\langle v_x \rangle_u$ as their parents are themselves likely to fragment. If, however, the child has the opposite sign of $\langle v_x \rangle_u$ to that of the parent the child most likely dissolves. Thus the offspring inheriting the main features of the velocity field of the parent are more likely to fragment. Note that the fragmenters in Fig. 17c lie closer to the solid line than the dissolvers.

5. Discussion and conclusions

We have presented the results of a 2-D, fully compressible radiation-hydrodynamic simulation. The computational domain (with a horizontal extent of over 17 Mm) harbours more than a dozen granules at any given time. In addition, the simulation has been run for approximately 5 solar hours. As result the evolution of over 400 granules could be followed allowing us to carry out a statistical analysis, giving new insight into the temporal evolution averaged over many granules. We acknowledge that the limitation to two spatial dimensions may restrict the generality of the conclusions somewhat, but we expect that the main conclusions regarding the physical processes controlling granule evolution should remain valid in 3–D, although the number and relative importance of various physical processes will probably be different. Also, additional aspects may need to be considered in 3-D.

This simulation suggests a simple characterization into two types of granules (cf. Fig. 1): *fragmenting* granules end when a new downflowing lane forms in their interior, whereas *dissolving* granules contract until two embracing lanes merge together and the intervening granule disappears. In our simulation an equal number of granules die through fragmentation as through dissolution. A few examples of a third type of granule, namely merging granules, which end when two granules merge to form a new and larger granule, may be present, but due to ambiguity in identifying them we have not studied them in detail (cf. Sect. 3.2). The number of possible merging granules is negligible.

In order to investigate the temporal evolution averaged over many granules we average physical quantities (at fixed height and at a fixed stage of the granule's evolution) over the granule and over all granules of the same type at the same stage of the evolution. In the case of fragmenters, we additionally determine the evolution of different physical parameters along the locations at which the new downflow lane is formed during fragmentation.

We are well aware that by dividing granules strictly into two groups and considering only averaged quantities we have considerably simplified the often complex evolution of individual granules. For example, in a number of cases a young granule initially expands just like a normal fragmenter. At some point, however, its expansion is stopped by even stronger neighbouring granules. Eventually, the boundaries of this granule are pushed back again until it dies as a dissolver (into which category it also enters in this analysis). Such an example is found, e.g., in Fig. 1b at time $\mathcal{T} = 3\,\mathrm{h}\,10'$ and position 2 Mm.

The physical quantities averaged over a fragmenting granule give little warning of the impending fragmentation. However, at the location at which the fragmentation occurs and the new

lane is formed the signature of buoyancy braking is clearly seen. A local pressure excess compresses upflowing gas and decelerates it. Mass conservation then forces the horizontal flow speed at a greater height to be reduced. This in turn allows the gas to cool through radiative losses, thus increasing its density further, which finally reduces its buoyancy. The process leading to fragmentation first starts in the highest considered layers at the solar surface and later propagates down Hence the death of fragmenters (and the birth of new granules) is (statistically significantly) driven by surface phenomena.

In contrast to fragmenting granules, the spatially averaged pressure and temperature of dissolving granules decrease throughout their evolution, starting soon after birth. A decrease in vertical velocity and an increase in density is only seen much later, near dissolution. This behaviour can partly be understood by the decrease in size of granules and mass conservation, which leads to a proportional decrease of the horizontal velocity. The pressure excess that is built up during the temporal evolution, as required by the need to accelerate the matter to the maximum horizontal velocity, is proportional to the square of the granule's size. This makes the shrinking dissolving granules rapidly weaker relative to its neighbours in the sense that it has increasingly smaller relative pressure. This pressure difference between neighbouring granules is crucial and relates the evolution of both types of granules to each other. In fact, the combined evolution of a neighbouring pair of granules, a dissolver and a fragmenter, i.e. one granule that contracts and one that expands, can be considered to be a form of instability: As the dissolver contracts mass conservation requires less strong horizontal flows. Consequently, its pressure, required to accelerate such flows, decreases, which makes the pressure excess of the fragmenter relative to the dissolver even larger. This in turn causes the dissolver to contract even more rapidly and the fragmenter to expand similarly, and so on.

The evolution of granules is hence determined by the horizontal forces exerted by the granules on their neighbours. This behaviour had been predicted by Stein & Nordlund (1998). Note that the relative pressure difference between neighbouring granules is largest in the highest layer that we consider. Hence, for both fragmenters and dissolvers the surface layers are decisive for their evolution.

The dissolving granules are statistically born "weaker", i.e. they are cooler, denser and have lower pressure excess compared to the fragmenting granules. However, it is the size at birth that allows the most precise prediction of the fate of a granule. In our simulations granules are born almost exclusively by fragmentation, i.e. in general as twins. If one of the twins later dissolves and the other fragments, then in almost all cases it is the smaller one that dissolves. None of the other physical quantities predicts the later fate of a granule with the same accuracy, although fragmenting granules are on average also born hotter and with higher pressure then their dissolving counterparts.

A striking feature is that many dissolving granules have a horizontal velocity pointing in only one direction. Such dissolvers generally also do not possess a central pressure excess. Instead, a large pressure excess builds up over the intergranular lane lying between the increasingly weaker dissolver and a powerful neighbouring granule.

Let us briefly consider some of the differences that we expect between our 2–D simulation and three dimensional reality. For one, intergranular lanes are spatially unconnected in 2–D, whereas they form a network in 3–D. This also means that whereas in 2–D a small, weak granule caught between two large powerful granules cannot escape and is finally crushed between them (i.e. it dissolves), in 3–D it may escape by squeezing out to the side. If this is the case dissolution as a means of death would be less common in 3–D. On the other hand, it may be easier to make a intergranular lane disappear in 3–D than in 2–D. If, e.g. in 2–D a strong upwelling starts below an intergranular lane, then it will probably push the lane to one side, but not destroy it, and the lane will in most cases survive intact. The reason is that since lanes are isolated in 2-D, unless the horizontal flows in the immediate vicinity of a lane change sign a downflow there will be needed to return that material to the solar interior upon disappearance of the lane. In 3–D, however, such an upwelling can part a downflow lane from below like a pair of curtains, effectively producing a new granule by merging two neighbours. Such effects could explain why the ratio of dissolving to merging granules is so much larger in 2–D than observed by Mehltretter (1978).

Finally, we point out that in 2-D the horizontal velocities in granules are larger than in 3-D. Hence the pressure difference between large and small granules may be smaller in 3-D than we find here. This effect may also help to reduce the number of dissolving granules relative to merging granules.

Acknowledgements. This work has been supported by grants No. 20-43048.95 of the Swiss National Science Foundation. We thank A. Hanslmeier, K.N. Pikalov and K.G. Pushmann for their help in carrying out the computations. S.R.O. Ploner thanks P.N. Bernasconi for the help with the figures.

References

Amsden A. A., 1966, Los Alamos Rept. No. LA-3466, Los Alamos Scientific Laboratory, Los Alamos, New Mexico
Atroshchenko I. N., Gadun A. S., 1994, A&A 291, 635
Belocerkovskij O. M., Davydov Yu. M., 1982, The Large-Particle Method (in russian), Nauka, Moscow
Deubner F.-L., Fleck B., Marmolino C., Severino G., 1990, A&A 236, 509
Dialetis D., Macris C., Prokakis T., Sarris E., 1986, A&A 168, 330
Dravins D., Lindegren L., Nordlund Å., 1981, A&A 96, 345
Dravins D., Larsson B., Nordlund Å., 1986, A&A 158, 83
Freytag B., Ludwig H.-G., Steffen M., 1996, A&A 313, 497
Gadun A. S., 1995, Kinematika i Fisika Nebesnukh Tel 11, 54
Gadun A. S., Vorob'yov Yu. Yu., 1995, Sol. Phys. 159, 45
Gadun A. S., Pikalov K. N., 1996, Sol. Phys. 166, 43
Gadun A. S., Hanslmeier A., Pikalov K. N., 1997, A&A 320, 1001
Gadun A. S., Solanki S. K., Johannesson A., 1998a A&A, in press
Gadun A. S., Solanki S. K., Ploner S. R. O. et al., 1998b Preprint, Nas Ukraine, MAO-98-4E, MAO, Kiev
Hirzberger J., Vázquez M., Bonet J. A., Hanslmeier A., Sobotka M., 1997, ApJ 480, 406
Hurlburt N. E., Toomre J., Massaguer M., 1984, ApJ 282, 557

Karpinsky V. N., Pravdjuk L. M., 1998, Kinematika i Fizika Nebesnukh Tel 14 (2), 119
Kawaguchi I., 1980, Sol. Phys. 65, 207
Kurucz R. L., 1979, ApJSS 40, 1
Latour J., Toomre J., Zahn J.-P., 1983, Sol. Phys. 82, 387
Lites B. W., Nordlund Å., Scharmer G. B., 1989, in Solar and Stellar Granulation, R. J. Rutten, G. Severino (Eds), Kluwer, Dordrecht, p. 349
Massaguer J. M., Zahn J.-P., 1980, A&A 87, 315
Mehltretter J. P., 1978, A&A 62, 311
Muller R., 1989, in Solar and Stellar Granulation, R.J. Rutten, G. Severino (Eds.), Kluwer, Dordrecht, p. 101
Nordlund Å., 1985, Sol. Phys. 100, 209
Nordlund Å., Spruit H. C., Ludwig H.-G., Trampedach R., 1997, A&A 328, 229
Ploner S. R. O., Solanki S. K., Gadun A. S., Hanslmeier A., 1998, Space Sci. Rev. 85, 261
Rast M. P., 1995, ApJ 443, 863
Rast M. P., 1999, in Geophysical and Astrophysical Convection, P. Fox and R. Kerr (Eds.), Gordon and Breach Publishers, in press
Schüssler M., 1992, in The Sun - a Laboratory for Astrophysics, J. T. Schmelz and J. C. Brown (Eds.), Kluwer, Dordrecht, p. 81
Spruit H. C., 1997, Mem. S. A. It. 68, 397
Spruit H. C., Nordlund Å., Title A. M., 1990, ARA&A 28, 263
Steffen M., Ludwig H.-G., Krüß A., 1989, A&A 213, 371
Stein R. F., Nordlund Å., 1989, ApJ 342, L95
Stein R. F., Nordlund Å., 1994, in Infrared Solar Physics, D. M. Rabin, J. T. Jefferies, C. Lindsey (Eds.), Kluwer, Dordrecht, p. 225
Stein R. F., Nordlund Å., 1998, ApJ 499, 914
Title A.M., Tarbell T.D., Simon G.W., et al., 1986, Adv. Space Res. 6, 253
Title A.M., Tarbell T.D., Topka K.P. et al., 1989, ApJ 336, 475
Wöhl H., Nordlund Å., 1985, Sol. Phys. 97, 213